Acoustic scattering from density and sound speed gradients: Modeling of oceanic pycnoclines

Tetjana Ross
Department of Oceanography, Dalhousie University, Halifax, Nova Scotia B3H 4R2, Canada
tetjana@dal.ca

Andone C. Lavery
Applied Ocean Physics and Engineering, Woods Hole Oceanographic Institution, Woods Hole, Massachusetts 02543
alavery@whoi.edu

Abstract: A weak-scattering model that allows prediction of acoustic scattering from oceanic pycnoclines (and the accompanying sound speed gradients) based on hydrographic profiles is described. Model predictions, based on profiles from four locations, indicate that scattering from oceanic pycnoclines is measurable using standard scientific sonars operating at frequencies up to 200 kHz but generally only for pycnocline thicknesses less than 10 m. Accurate scattering models are key to assessing whether acoustic remote sensing can be used to map oceanic pycnoclines and for determining whether scattering from pycnoclines needs to be taken into account when estimating, for instance, zooplankton abundance from acoustic data.

PACS numbers: 43.30.Gv, 43.30.Ft [JL]
Date Received: August 31, 2011 **Date Accepted:** November 21, 2011

1. Introduction

Pycnoclines are important oceanographically (e.g., Mann and Lazier, 2006), and there is a long history of observations (e.g., Fisher and Squier, 1975; Penrose and Beer, 1981) of enhanced acoustic scattering at mid (1–10 kHz) and high frequencies (>10 kHz) associated with oceanic pycnoclines, defined as gradients in density, but which in the following discussion also refer to the accompanying sound speed gradients. The possibility of scattering from oceanic sound speed gradients was suggested decades ago (Munk and Garrett, 1973) and, around the same time, a scattering model that included sound speed and density gradients was developed (Gupta, 1966). This scattering model is complex to implement, and applying it to pycnoclines requires making assumptions about the processes giving rise to the pycnoclines (Penrose and Beer, 1981). Penrose and Beer (1981) used it, however, to conclude that scattering at 200 kHz observed at an estuarine salt wedge was due to the pycnocline and not suspended sediments. More generally it is typically assumed that the observed scattering associated with oceanic pycnoclines is due to passive particulate tracers (Kaye and Anderson, 1979), such as zooplankton or suspended sediments.

This work presents a simple, physics-based, weak-scattering model for scattering from density and sound speed gradients with applications to oceanic pycnoclines. This model is based on a weak-scattering model initially developed to describe scattering from double-diffusive interfaces (Lavery and Ross, 2007), is easy to implement, and does not require assumptions about the physical processes behind the formation and maintenance of the pycnocline.

2. Weak-scattering model for oceanic pycnoclines

Double-diffusive interfaces are a special case of an oceanic pycnocline with very sharp gradients. Lavery and Ross (2007) have developed an acoustic backscattering model

for double-diffusive interfaces in which the interface is divided into thin sublayers, each with a constant sound speed and density. The scattering from each sublayer is assumed to be dominated by a single scattering event and added coherently. The density and sound speed associated with the interface can be described by idealized forms or measured profiles [Fig. 1(a)]. The ratio of the scattered pressure P_{scat} to the incident pressure P_{inc}, in the far field, is given by [Eq. (9); Lavery and Ross, 2007]

$$\frac{P_{scat}}{P_{inc}} = \frac{1}{2}\left[R_{I,1} + \sum_{n=1}^{N} R_{n,n+1} \exp\left(2i \sum_{m=1}^{n} k_m \Delta\right)\right], \tag{1}$$

where Δ is the thickness of the homogeneous sublayers (chosen to be at least 20 times smaller than the acoustic wavelength), N is the number of sublayers, and k_m is the acoustic wavenumber in sublayer m. The R's are reflection coefficients, e.g., $R_{n,n+1} = (\rho_{n+1}c_{n+1} - \rho_n c_n)/(\rho_{n+1}c_{n+1} + \rho_n c_n)$, where ρ_n is the density and c_n is the sound speed in the sublayer n. The properties of the homogeneous layer above the pycnocline (above sublayer 1) are given by the subscript I, and those of the homogeneous layer below the pycnocline (below sublayer N) are indicated by the subscript II, and $R_{N,N+1} \equiv R_{N,II}$.

The assumption that the spatial extent of the pycnocline (Δz) is much less than the range to the pycnocline (r_{scat}), must be relaxed for oceanic pycnoclines:

$$\frac{P_{scat}}{P_{inc}} = \frac{1}{2}\left[R_{I,1} + \sum_{n=1}^{N} \frac{R_{n,n+1} \exp\left(2i \sum_{m=1}^{n} k_m \Delta\right)}{1 + \left(\sum_{m=1}^{n} \Delta\right) \Big/ r_{scat}}\right], \tag{2}$$

which is a slight rearrangement of Eq. (8) in Lavery and Ross (2007)

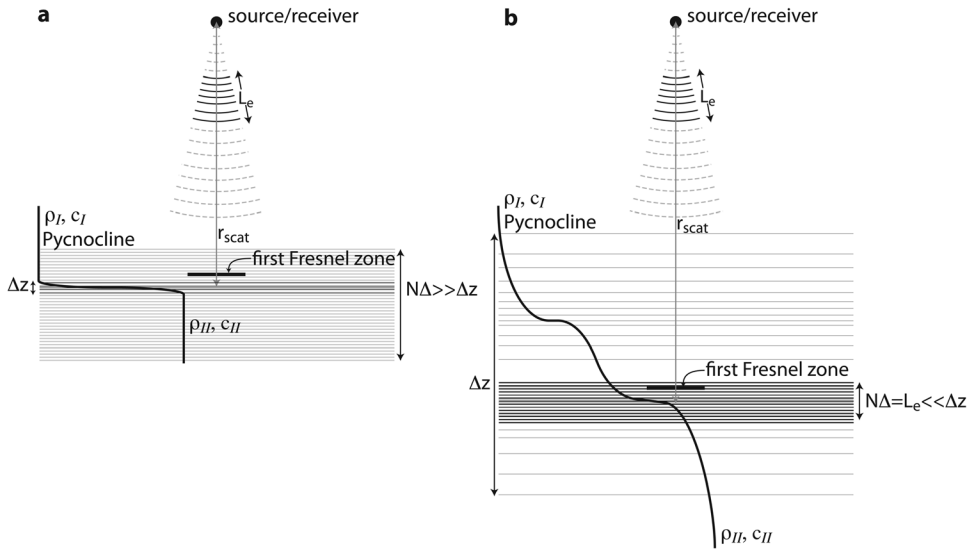

Fig. 1. Scattering geometry for (a) the double-diffusive (or very sharp pycnocline) and (b) the general pycnocline scattering model. The dotted lines show the sound emanating from the source/receiver, those that are solid indicate the length of the integration length scale, L_e. Horizontal lines are used to suggest the scattering surfaces implicit in the model formulation. The irregularly spaced lines [dark in (a) and light in (b)] illustrate the gradient in acoustic impedance over the interface thickness, Δz. The regularly spaced horizontal lines [light in (a) and dark in (b)] illustrate the regular spacing of the sublayers (Δ) within L_e.

Equation (1) also assumes that all the variability causing acoustic backscattering is contained within one echo integration length scale, L_e [i.e., $\Delta z \ll L_e$ as in Fig. 1(a)]. L_e refers to the spatial length scale associated with the segment of the raw measured voltage that is integrated over to obtain scattering strength for each range bin of each ping. In single-frequency echosounders, the integration length scale is typically the length of the transmitted pulse. Equations (1) and (2) discretely integrate over all of the variability, thus assuming L_e is infinite. This is a safe assumption as long as $\Delta z \ll L_e$, which was valid for double-diffusive interface laboratory scattering. It will also be valid for most double-diffusive pycnoclines, which typically have interface thicknesses around 10 cm, which is short compared to typical pulse (and thus integration) lengths of around 200 μs, or 30 cm, for high-frequency echosounders.

When the variability extends longer than L_e [e.g., Fig. 1(b)], then it is more appropriate to integrate over only the sublayers contained within one L_e. Given the assumption of weak-scattering, this can be done by replacing N with $N = L_e/\Delta$ and summing each integration length separately. For the Mth segment, spanning $(M-1)L_e + \Delta$ to ML_e,

$$\frac{P_{scat}}{P_{inc}}(M) = \frac{1}{2}\sum_{n=(M-1)N}^{MN} \frac{R_{n,n+1}\exp\left(2i\sum_{m=(M-1)N}^{n} k_m\Delta\right)}{1+\sum_{m=(M-1)N}^{n}\Delta/r_{scat}}, \tag{3}$$

which assumes that only the phase changes over the integration length scale is important. Also, the $R_{I,1}$ term in Eq. (2) has been wrapped into the sum by starting the sum at $(M-1)N$ rather than $(M-1)N+1$ (i.e., starting at 0 rather than 1 for $M=1$ with the assumption that $R_{0,1} \equiv R_{I,1}$).

In the double-diffusive interface scattering model, r_{scat} is the distance to the interface. For an extended pycnocline, being represented as a series of sums over range segments of length L_e, r_{scat} should be different for each segment. Taking the Mth r_{scat} to be the middle of that range segment, $r_{scat}(M) = (M-1/2)L_e$. Thus, $MN = (N/L_e)r_{scat}(M) + N/2 = r_{scat}\ (M)/\Delta + N/2$, and $(M-1)N = r_{scat}(M)/\Delta - N/2$. This can be used to simplify the sum in the denominator and dropping the $r_{scat}(M)$ notation, Eq. (3) then becomes

$$\frac{P_{scat}}{P_{inc}}(r_{scat}) = \frac{1}{2}\sum_{n=r_{scat}/\Delta-N/2}^{r_{scat}/\Delta+N/2} \frac{R_{n,n+1}\exp\left(2i\sum_{m=r_{scat}/\Delta-N/2}^{n} k_m\Delta\right)}{\left(n+\frac{N}{2}+1\right)\Delta/r_{scat}}, \tag{4}$$

which is now explicitly a function of range. The reflection coefficients can be calculated from a measured profile of any shape and no assumptions about the processes creating the pycnocline need to be made, making Eq. (4) more comprehensive and simpler to implement than the Gupta (1966) and Penrose and Beer (1981) models.

To facilitate comparison with scattering from discrete targets (such as zooplankton), it is useful to express the pycnocline scattering in terms of volume scattering strength, S_v in dB re 1 m^{-1}. S_v is given by (Ross and Lavery, 2010),

$$S_v = 10log_{10}\left(\frac{\left(\frac{P_{scat}}{P_{inc}}\right)^2}{2\pi L_e(1-cos(\theta_{1/2}))}\right), \tag{5}$$

where the sampling volume at the range r_{scat} has been approximated as $2\pi L_e r_{scat}^2(1-\cos(\theta_{1/2}))$ and $\theta_{1/2}$ is the angle (in radians) of the half-beam width of a conical beam.

3. Model predictions for oceanic pycnoclines

3.1 Predictions based on hydrographic profiles

To illustrate the potential scattering strength from realistic oceanic pycnoclines, the temperature (T) and salinity (S) profiles from four locations were fit to a physics-based functional form for thermo- and halo-clines [Eq. (1) in González-Pola *et al.*, 2007] [Figs. 2(a) and 2(b)]. From this, theoretical density and sound speed profiles for each of these locations were calculated [Figs. 2(c) and 2(d)] and used in the pycnocline scattering model [Eq. (4); Figs. 2(e) and 2(f)]. S_v at 38 kHz [upper axis of Fig. 2(e)] were estimated using $\theta_{1/2}=3.5^\circ$ and $L_e=0.38$ m, which is based on the system parameters for the common commercial Simrad 38-7 sonar.

The frequency dependence of the predicted scattering is dominated by an oscillatory pattern, as in Lavery and Ross (2007), resulting from constructive and destructive interference related to the thickness of the interface, Δz. For these examples, however, $L_e<\Delta z$ and thus L_e controls the spacing of the nulls by setting a limit on the number of wave cycles that are summed.

For pycnocline scattering to be measurable, it must at least exceed the noise-floor of the sonar system (often around -100 dB or $P_{scat}/P_{inc}=10^{-6}$ for the sonar

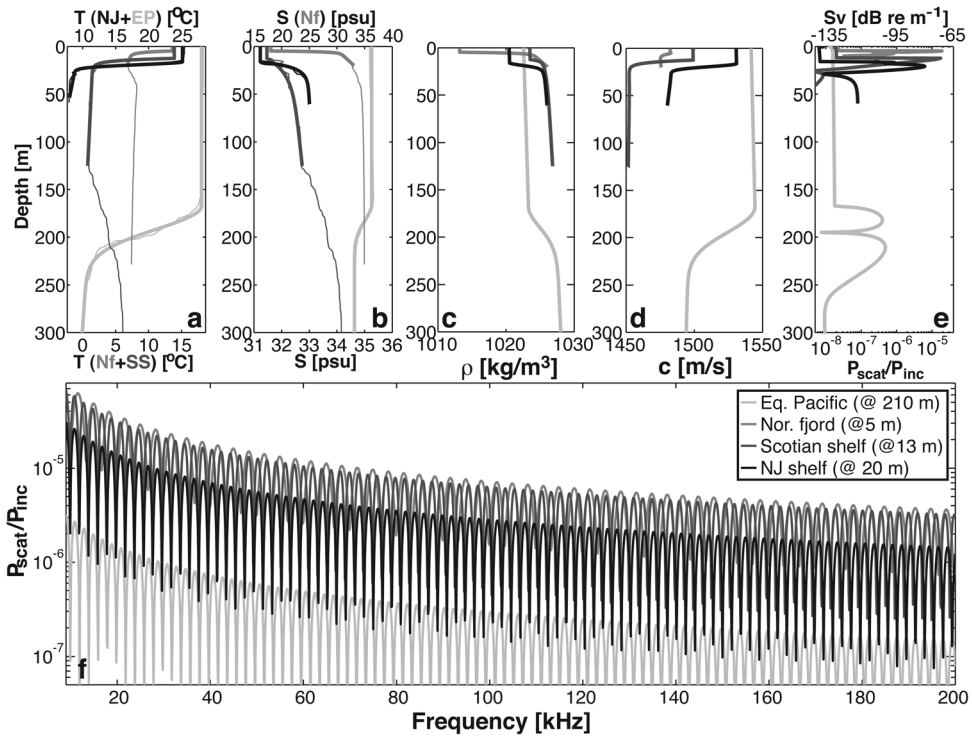

Fig. 2. Examples of applying the pycnocline scattering model, Eq. (4), by fitting the González-Pola *et al.* (2007) model to profiles collected in the Equatorial Pacific (EP), the Scotian shelf (SS), a Nowegian fjord (Nf), and the New Jersey continental shelf (NJ). (a) Temperature profiles (thin lines) and the theoretical fit (thick lines). (b) Same as (a), but for salinity. (c) Density profiles calculated from theoretical profiles shown in (a) and (b). (d) Sound speed profiles calculated from theoretical profiles shown in (a) and (b). (e) Predicted volume scattering strength at 38 kHz as a function of depth for the theoretical profiles shown in (c) and (d). (f) Predicted scattering (scattered pressure) at the pycnocline depth (indicated in the legend) as a function of frequency. Scattering predictions are based on the functional fits evaluated with a vertical resolution of 0.75 mm.

parameters used here). Scattering is predicted at measurable levels at 38 kHz [Fig. 2(e)] and even up to 200 kHz [Fig. 2(f)] for both continental shelf profiles, with strong seasonal thermoclines, and for the Norwegian fjord, with its strong halocline. Note that similar levels of scattering are predicted for the Norwegian fjord (with a large density gradient and relatively small sound speed gradient) and the Scotian shelf (with a small density gradient and large sound speed gradient). While it has the largest temperature step across it, predicted scattering for the Equatorial Pacific profile is negligible as the gradients are too weak.

3.2 Scattering dependence on ΔT *and* ΔS

Figure 3 explores the effect of varying the T and S steps (and hence the ρ and c steps) on the predicted pycnocline volume scattering strengths (using the system parameters given in the preceding text). A theoretical pycnocline, with shape parameters taken from the fit to the New Jersey shelf profiles, was calculated for each set of surface values. The depth of the pycnocline was fixed at 30 m, the deep layer T and S were fixed at 5 °C and 35 psu, respectively, and the surface T and S varied over a realistic range (effectively varying ΔT and ΔS). Note, however, that due to the saddle point in $\rho(T)$, the dependence of volume scattering on surface temperature also depends on bottom temperature. The predicted scattering is largest for the warmest surface temperatures (i.e., the largest ΔT) and freshest surface salinities (i.e., the largest ΔS). Low scattering predictions extend from small ΔT and ΔS along lines where ρ and c changes have opposing effects on the acoustic impedance change across the pycnocline.

In the ocean, many of the parameters needed for the pycnocline scattering model do not vary independently. T and S (as well as pressure) determine both ρ and c, and not only do they typically vary only over certain ranges, they are often linked (T-S relationships are often used to identify water masses, e.g., Pickard and Emery, 1990). Near the 4 °C low point in saltwater density, the same ΔT can lead to

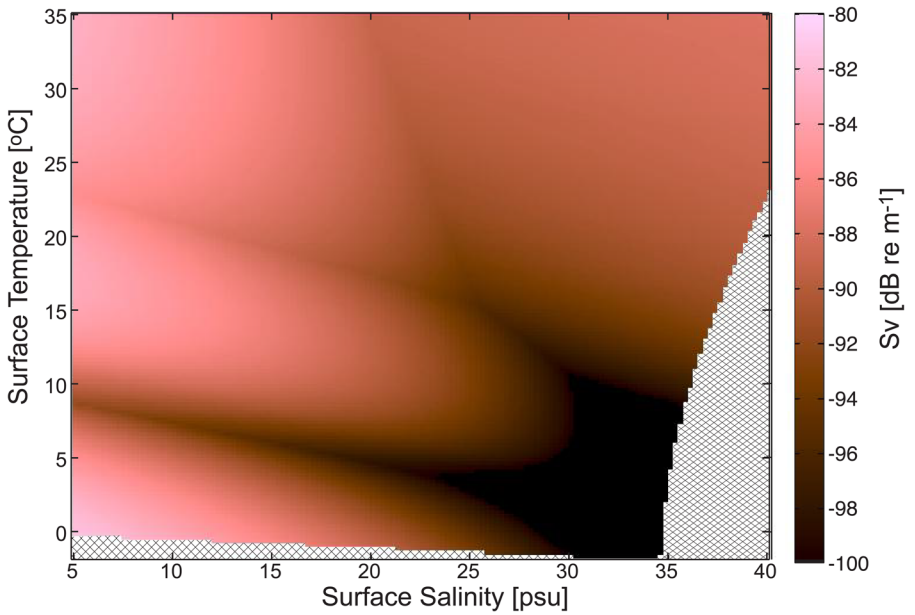

Fig. 3. (Color online) A false color map of predicted pycnocline S_v at 38 kHz as a function of surface T and S. The pycnocline scattering model is applied to density and sound speed profiles calculated from shape parameters based on the New Jersey shelf data. The T and S steps across pycnoclines of fixed depth (30 m) and thickness ($\Delta z \approx 10$ m) were varied. The hatched area in the bottom left is where the surface water would freeze, and the one on the right is where the density profiles would be unstable.

opposite changes in density. Furthermore, it is possible for the steps in T and S to lead to equal and opposite changes in acoustic impedance (ρc) because of opposite changes in ρ and c. Also, the sharpness of the interface will be related to the density step across it. Because pycnoclines with large density steps require more energy to mix, they are likely to have a different distribution of thicknesses (i.e., they may be thinner). Ideally, pycnocline scattering will be predicted from actual profiles, so this dependence need not be parameterized.

3.3 Model limitations

Although pycnoclines are assumed to be smooth in this model, roughness on some scales inevitably occurs. It is worthwhile considering what limits of roughness do not violate the model assumptions. In the vertical, as discussed in Lavery and Ross (2007), if the root-mean-square height of roughness on the interface is less than the wavelength of sound, the interface is well modeled as a smooth surface. In the horizontal, the area of an element roughness must occupy a considerable fraction of the first Fresnel zone to appear smooth (Mahoney *et al.*, 1973). Thus, roughness with a small vertical dimension (relative the the wavelength) or a large horizontal dimension (relative to the first Fresnel zone), such as undulations in the pycnocline, does not violate the model assumptions. The first Fresnel radius is given by $\sqrt{\lambda r_{scat}/2}$, so for the example of 38 kHz sound, the pycnocline surfaces would have to be smooth on the horizontal scale of only 14 cm at 1 m range, 44 cm at 10 m range, and 140 cm at 100 m range.

The discussion to date has also assumed that a high-resolution profile (i.e., $\lambda/20$) is available, so that all the relevant scales of density and sound speed gradients can be included in the summation. For high frequencies, this requires specialized microstructure observations, and for frequencies beyond about 200 kHz, it is not feasible to make *in situ* temperature and salinity measurements at the $\lambda/20$ scale.

4. Conclusions

A weak-scattering model for double-diffusive interfaces has been generalized to be applicable for a wider range of pycnocline thicknesses. This simple, easy-to-use model allows the use of measured hydrographic profiles to predict the scattering. The model was applied to four example hydrographic profiles, and measurable scattering was predicted up to 200 kHz for pycnocline thicknesses $\leq$10 m, regardless of whether the density/sound speed step was predominantly due to a temperature or a salinity step. Strong pycnoclines are not uncommon in the ocean, particularly in coastal areas with significant freshwater input and during the peak of the seasonal thermocline. This model provides a simple means of evaluating whether pycnoclines could be observable acoustically. This will benefit both researchers seeking to study pycnoclines and those interested in their passive tracers.

Acknowledgments

We thank Jim Moum for the NJ profile and www.nodc.noaa.gov for the others.

References and links

Fisher, F. H., and Squier, E. D. (**1975**). "Observation of acoustic layering and internal waves with a narrow-beam 87.5-khz echo sounder," J. Acoust. Soc. Am. **58**, 1315–1317.

González-Pola, C., Fernández-Díaz, J. M., and Lavín, A. (**2007**)."Vertical structure of the upper ocean from profiles fitted to physically consistent functional forms," Deep-Sea Res. I **54**, 1985–2004.

Gupta, R. N. (**1966**). "Reflection of sound waves from transition layers," J. Acoust. Soc. Am. **39**, 255–260.

Kaye, G. T., and Anderson, V. C. (**1979**)."Scattering from oceanic microstructure: Detection with a large aperture array," J. Acoust. Soc. Am. **66**, 842–849.

Lavery, A., and Ross, T. (**2007**). "Acoustic scattering from double-diffusive microstructure," J. Acoust. Soc. Am. **122**, 1449–1462.

Mahoney, A. R., Gage, K., Ottersten, H., and Tennekes, H. (**1973**). "The interaction between atmospheric microstructure and acoustic and electromagnetic waves," Boundary-Layer Meteorol. **5**, 219–226.

Mann, K. H., and Lazier, J. R. N. (**2006**). *Dynamics of Marine Ecosystems: Biological-Physical Interactions in the Oceans*, 3rd ed. (Blackwell Publishing Ltd., Malden, MA).
Munk, W., and Garrett, C. (**1973**). "Internal wave breaking and microstructure (the chicken and the egg)," Boundary-Layer Meteorol. **4**, 37–45.
Penrose, J. D., and Beer, T. (**1981**). "Acoustic reflection from estuarine pycnoclines," Estaurine Coastal Shelf Sci. **12**, 237–249.
Pickard, G. L., and Emery, W. J. (**1990**). *Descriptive Physical Oceanography: An Introduction*, 5th ed. (Butterworth-Heinemann Ltd., Oxford, UK), pp. 144–152 and 204–207.
Ross, T., and Lavery, A. (**2010**). "Acoustic detection of oceanic double-diffusive convection: A feasibility study," J. Atmos. Ocean. Tech. **27**, 580–593.